

# Measured double-pass intensity point-spread function after adaptive optics correction of ocular aberrations

Eric Logean, Eugénie Dalimier, and Chris Dainty

*Applied Optics Group, National University of Ireland, Galway, University Rd, Galway, Ireland*

[eric.logean@nuigalway.ie](mailto:eric.logean@nuigalway.ie)

<http://optics.nuigalway.ie>

**Abstract:** The double-pass intensity point-spread function was recorded in four subjects using a monochromatic source emitting at 543 nm, through a 6.7-mm diameter pupil i) at the fovea after adaptive optics correction of the ocular aberrations, ii) at the fovea without adaptive optics correction, and iii) at 2° of eccentricity with adaptive optics correction. The half-width at half-maximum of the double-pass point-spread function was narrower after correction of the ocular aberrations. At 2° of eccentricity this width was larger than at the fovea. The minimum widths were about 1.1 arcmin in dark pigmented eyes and 1.6 arcmin in light pigmented eyes. These values are 6 to 9 times larger than the width expected from diffraction alone.

© 2008 Optical Society of America

**OCIS codes:** (110.1080) Adaptive optics; (170.0110) Imaging systems; (170.4460) Ophthalmic optics and devices.

---

## References and links

1. J. Liang, D. R. Williams, and D. T. Miller, "Supernormal Vision and High-Resolution Retinal Imaging through Adaptive Optics," *J. Opt. Soc. Am. A* **14**, 2884–2892 (1997).
2. A. Roorda and D. R. Williams, "The Arrangement of the Three Cone Classes in the Living Human Eye," *Nature* **397**, 520–522 (1999).
3. J. Rha, R. S. Jonnal, K. E. Thorn, J. Qu, Y. Zhang, and D. T. Miller, "Adaptive Optics Flood-Illumination Camera for High Speed Retinal Imaging," *Opt. Express* **14**, 4552–4569 (2006).
4. A. W. Dreher, J. F. Bille, and R. N. Weinreb, "Active Optical Depth Resolution Improvement of the Laser Tomographic Scanner," *Appl. Opt.* **28**, 804–808 (1989).
5. A. Roorda, F. Romero-Borja, W. J. Donnelly III, H. Queener, T. J. Herbert, and M. C. W. Campbell, "Adaptive Optics Scanning Laser Ophthalmoscopy," *Opt. Express* **10**, 405–412 (2002).
6. S. A. Burns, R. Tumbar, A. E. Elsner, D. Ferguson, and D. X. Hammer, "Large-Field-of-View, Modular, Stabilized, Adaptive-Optics-Based Scanning Laser Ophthalmoscopy," *J. Opt. Soc. Am. A* **24**, 1313–1326 (2007).
7. B. Hermann, E. J. Fernández, A. Unterhuber, H. Sattmann, A. F. Fercher, W. Drexler, P. M. Prieto, and P. Artal, "Adaptive-Optics Ultrahigh-Resolution Optical Coherence Tomography," *Opt. Lett.* **29**, 2142–2144 (2004).
8. Y. Zhang, J. Rha, R. S. Jonnal, and D. T. Miller, "Adaptive Optics Parallel Spectral Domain Optical Coherence Tomography for Imaging the Living Retina," *Opt. Express* **13**, 4792–4811 (2005).
9. R. J. Zawadzki, S. M. Jones, S. S. Olivier, M. Zhao, B. A. Bower, J. A. Izatt, S. Choi, S. Laut, and J. S. Werner, "Adaptive-Optics Optical Coherence Tomography for High-Resolution and High-Speed 3D Retinal In Vivo Imaging," *Opt. Express* **13**, 8532–8546 (2005).
10. D. Merino, C. Dainty, A. Bradu, and A. G. Podoleanu, "Adaptive Optics Enhanced Simultaneous En-Face Optical Coherence Tomography and Scanning Laser Ophthalmoscopy," *Opt. Express* **14**, 3345–3353 (2006).
11. M. Glanc, E. Gendron, F. Lacombe, D. Lafaille, J.-F. L. Gargasson, and P. Léna, "Towards Wide-Field Retinal Imaging with Adaptive Optics," *Opt. Commun.* **230**, 225–238 (2004).
12. F. Flamant, "Étude de la Répartition de Lumière dans l'Image Rétinienne d'une Fente," *Rev. Opt. Theor. Instrum.* **34**, 433–459 (1955).

13. G. Westheimer and F. W. Campbell, "Light Distribution in the Image Formed by the Living Human Eye," *J. Opt. Soc. Am.* **52**, 1040–1045 (1962).
14. F. W. Campbell and R. W. Gubisch, "Optical Quality of the Human Eye," *J. Physiol. (Lond.)* **186**, 558–578 (1966).
15. J. Santamaría, P. Artal, and J. Bescós, "Determination of the Point-Spread Function of Human Eyes using a Hybrid Optical-Digital Method," *J. Opt. Soc. Am. A* **4**, 1109–1114 (1987).
16. J. Liang and G. Westheimer, "Optical Performances of Human Eyes Derived from Double-Pass Measurements," *J. Opt. Soc. Am. A* **12**, 1411–1416 (1995).
17. J. Liang and D. R. Williams, "Aberrations and Retinal Image Quality of the Normal Human Eye," *J. Opt. Soc. Am. A* **14**, 2873–2883 (1997).
18. D. R. Williams, D. H. Brainard, M. J. McMahon, and R. Navarro, "Double-Pass and Interferometric Measures of the Optical Quality of the Eye," *J. Opt. Soc. Am. A* **11**, 3123–3135 (1994).
19. P. Rodríguez and R. Navarro, "Double-Pass versus Aberrometric Modulation Transfer Function in Green Light," *J. Biomed. Opt.* **12**, 044,018 (2007).
20. L. Diaz-Santana, C. Torti, I. Munro, P. Gasson, and C. Dainty, "Benefit of Higher Closed-Loop Bandwidths in Ocular Adaptive Optics," *Opt. Express* **11**, 2597–2605 (2003).
21. S. R. Chamot, C. Dainty, and S. Esposito, "Adaptive Optics for Ophthalmic Applications using a Pyramid Wave-front Sensor," *Opt. Express* **14**, 518–526 (2006).
22. E. Logean and C. Dainty, "Adaptation of the Zernike's Phase Contrast Method for Retinal Imaging," in *The Frontiers in Optics 2007/Laser Science XXIII*, OSA Technical Digest (CD), (Optical Society of America, 2007), paper JWC45.
23. E. Logean and C. Dainty, "Imaging of Phase Objects," (2008). European Patent # EP1964510 (A1).
24. E. Dalimier, K. M. Hampson, and J. C. Dainty, "Effects of Adaptive Optics on Visual Performance," in *Proc. SPIE: Opto-Ireland 2005: Imaging and Vision*, F. D. Murtagh, ed., vol. 5823, pp. 20–28 (2005).
25. E. Dalimier and C. Dainty, "Comparative Analysis of Deformable Mirrors for Ocular Adaptive Optics," *Opt. Express* **13**, 4275–4285 (2005).
26. American National Standard Institute, *American National Standard for Safe Use of Lasers*, Z136.1-2000 (Laser Institute of America, Orlando, USA, 2000).
27. D. J. Lund, P. Edsall, B. E. Stuck, and K. Schulmeister, "Variation of Laser-Induced Retinal Injury Thresholds with Retinal Irradiated Area: 0.1-s Duration, 514-nm Exposures," *J. Biomed. Opt.* **12**, 024,023 (2007).
28. P. Artal, S. Marcos, R. Navarro, and D. R. Williams, "Odd Aberrations and Double-Pass Measurements of Retinal Image Quality," *J. Opt. Soc. Am. A* **12**, 195–201 (1995).
29. L. Diaz-Santana and J. C. Dainty, "Effects of Retinal Scattering in the Ocular Double-Pass Process," *J. Opt. Soc. Am. A* **18**, 1437–1444 (2001).
30. F. C. Delori and K. P. Pflibsen, "Spectral Reflectance of the Human Ocular Fundus," *Appl. Opt.* **28**, 1061–1077 (1989).
31. W. J. Geeraets, R. C. Williams, G. Chan, J. W. T. Ham, D. G. III, and F. H. Schmidt, "The Relative Absorption of Thermal Energy in Retina and Choroid," *Invest. Ophthalmol.* **1**, 340–347 (1962).
32. M. J. Hogan, J. A. Alvarado, and J. E. Weddell, *Histology of the Human Eye: An Atlas and Textbook* (W. B. Saunders Company, Philadelphia, USA, 1971).
33. J. J. Vos and M. A. Bouman, "Contribution of the Retina to Entoptic Scatter," *J. Opt. Soc. Am.* **54**, 95–100 (1964).
34. R. Zeimer, M. Shahidi, M. Mori, S. Zou, and S. Asrani, "A New Method for Rapid Mapping of the Retinal Thickness at the Posterior Pole," *Invest. Ophthalmol. Vis. Sci.* **37**, 1994–2001 (1996).
35. J. J. Weiter, F. C. Delori, G. L. Wing, and K. A. Fitch, "Retinal Pigment Epithelial Lipofuscin and Melanin and Choroidal Melanin in Human Eyes," *Invest. Ophthalmol. Vis. Sci.* **27**, 145–152 (1986).
36. C. A. Curcio, K. R. Sloan, R. E. Kalina, and A. E. Hendrickson, "Human Photoreceptor Topography," *J. Comp. Neurol.* **292**, 497–523 (1990).
37. E. Logean, E. Dalimier, and C. Dainty, "Double Pass Intensity Images of a Point Source after Adaptive Optics Correction of Ocular Aberrations," in *Invest. Ophthalmol. Vis. Sci.* **49**, ARVO E-Abstract 4196 (2008).
38. G. J. van Blokland and D. van Norren, "Intensity and Polarization of Light Scattered at Small Angles from the Human Fovea," *Vision Res.* **26**, 485–494 (1986).
39. J. M. Gorrard, R. Alfieri, and J.-Y. Boire, "Diffusion of the Retinal Layers of the Living Human eye," *Vision Res.* **24**, 1097–1106 (1984).

## 1. Introduction

There has been tremendous interest in the limiting factors affecting retinal imaging since the introduction of adaptive optics (AO) to the flood illuminated fundus camera [1–3], confocal scanning laser ophthalmoscope [4–6], and optical coherence tomography (OCT) [7–10]. The performance of these AO systems are usually derived from the ocular aberrations measured by

the wavefront sensor (WS). Impressive reduction of the wavefront aberrations, tightening of the reconstructed point-spread function (PSF), and increase of the corresponding Strehl ratio were reported. These changes, however, reflect changes brought to the wavefront aberrations as measured by the WS and they may not reflect the changes brought to the retinal images. When the spatial frequency content of the retinal images is analysed [11], an increase is found in the magnitude of the mid-range frequencies for a given retinal area. This result reflects a real change in the retinal images obtained using AO.

Another approach is to measure the double-pass PSF, that is, to measure the light distribution in an image of the retina onto which a point source was imaged. This technique was used extensively to obtain the single-pass modulation transfer function of the eye at first using a slit source [12–14] and later using a point source [15–19], assuming a negligible contribution from the eye fundus, *i.e.*, that the eye fundus acts as a perfect single layer diffuser. The double-pass PSF is generally not measured in AO systems. Using a small entrance pupil and a large exit pupil, Diaz-Santana *et al.* [20] and Chamot *et al.* [21] showed the effect of AO correction on the double-pass PSF. The sensitivity of these measurements were limited by the small input pupil.

In the development of a coherent retinal imaging system [22,23], we assessed the feasibility of creating a point-like source at the fundus. We obtained, in young subjects, the double-pass PSF through a 6.7-mm diameter pupil after AO correction of the ocular aberrations. Here we report on the measured double-pass PSF and compare it to the uncorrected double-pass PSF, to the double-pass PSF reconstructed from the WS data and to the diffraction limited double-pass PSF. The measured double-pass PSF and the double-pass PSF reconstructed from the WS data should be similar provided that the light scattering within the eye is negligible.

## 2. Method

We built a fundus camera fitted with a closed-loop adaptive optics system. The main components of this camera are shown in Fig. 1. Starting from the subject's eye, the system consists of a telescopic arrangement (ophthalmic lens OL and lens L1) which images the pupil of the subject onto the deformable mirror (DM). After the DM, the optical system is separated in two parts by the dichroic beam splitter (DBS). One part is for wavefront sensing and the other part is for fundus imaging.

### 2.1. Closed-loop AO system

For wavefront sensing a 675-nm laser beam (B1) is focused on the eye fundus from a 1-mm diameter pupil located 2-mm off-axis ( $4\ \mu\text{W}$ ). The light back scattered from the fundus forms a wavefront at the exit pupil of the eye which is conjugated with the DM and the Hartmann–Shack WS. The wavefront is sampled by a grid of lenses (0.6-mm pitch at the cornea) which forms 97 spots onto a CCD camera (Retiga EX, QImaging, USA). The number of frames acquired per second ranged from 12 to 18. The WS data is converted, using the pseudo-inverse of the interaction matrix of the system [24], into the voltage commands used to control in closed-loop the 35-element bimorph DM (AOptix Inc, USA). The performance of this mirror to correct ocular aberrations was previously assessed [25].

### 2.2. Retinal imaging

For imaging, a 543-nm He-Ne laser beam B2 is used. This beam is reflected by the beam splitter BS2 and by the DBS. Then it is pre-corrected by the DM to form a sharply focused spot on the eye fundus. At the cornea, this beam has a power of 80 nW and enters the eye through a 6.7-mm diameter. The input pupil has a 2.6-mm diameter central obscuration to avoid light back-reflection from the optical elements of the system and from the optics of the subject eye. The

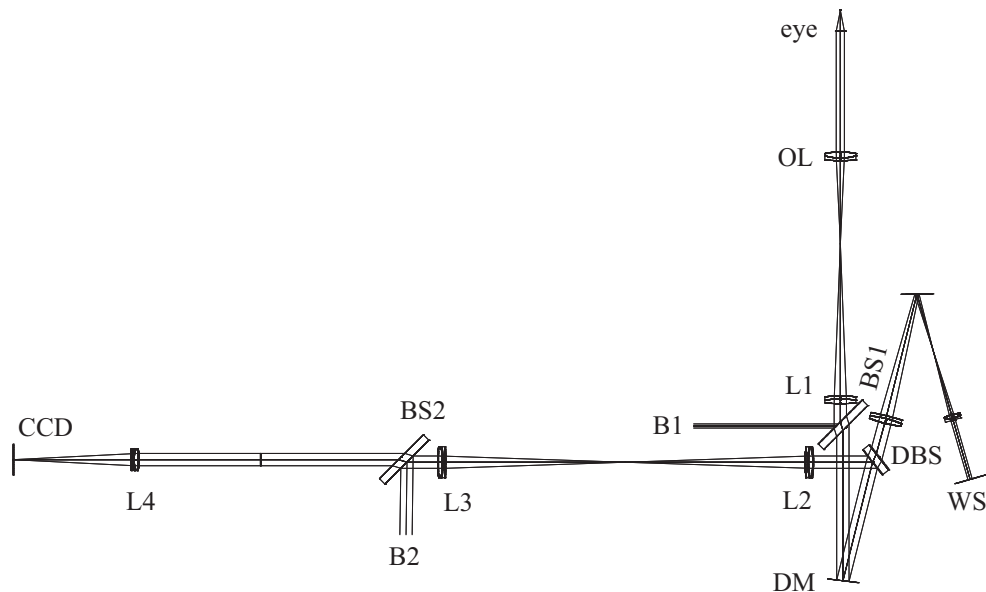


Fig. 1. Schematic drawing of the optical system, CCD charge coupled device, BS beam splitter (90 % transmission, 10 % reflection), DBS dichroic beam splitter, L lens, OL ophthalmic lens, B laser beams, DM deformable mirror, WS wavefront sensor

light back scattered by the fundus exits the eye through a 6.7-mm diameter clear aperture and it follows the same path up to the BS2, where it is transmitted toward the CCD camera (Rolera-XR, QImaging, USA). All the lenses of the system are achromats working at an F-number of 15. Each pixel of the camera subtends an angle of 0.20 minute of arc (arcmin) at the pupil of the eye ( $\approx 1 \mu\text{m}$  at the retina). By axially translating the lens L2, the conjugation of both the probing beam focused spot and the imaging CCD camera is changed. The lens L2 was adjusted to suppress the effect of the ocular longitudinal chromatic aberration and to obtain through focus double-pass PSF. A mechanical shutter (LST200, nmLaser Product, Inc, USA) limited the beam B2 exposure to 1 second. The retinal irradiance averaged over a circular area with a diameter equal to the full width at half maximum of the diffraction limited pattern (Airy disk) is 13 times less than the maximum permissible irradiance given by the ANSI standard [26]. The retinal irradiance was averaged over a smaller area than prescribed by the standard because the latter assume the presence of ocular aberrations [27].

### 2.3. Subjects and measurement protocols

Four subjects, one female and three males, aged between 25 and 36 years participated in this study. The two subjects A and B have darkly pigmented eyes and the two subjects C and D have lightly pigmented (blue) eyes. All eyes had spherical ametropia smaller than  $\pm 2$  dioptres and less than 1 dioptre of astigmatism. The measured eye was dilated using 1% Tropicamide drops.

We obtained three through focus series of double-pass PSF taken at five different focus depths (taken in a random order from -60, -30, 0, 30, 60  $\mu\text{m}$ , with 0  $\mu\text{m}$  being the focus position that gave the narrowest double-pass PSF in preliminary measurements in subject A). Series 1 was obtained with the beam aimed at the fovea after AO correction, Series 2 was obtained at the same location but without AO correction, and Series 3 was obtained at an angle of eccentricity of  $2^\circ$  ( $1.4^\circ$  nasally,  $1.4^\circ$  superior) with AO correction. For each series and at each focus depth three double-pass PSF were obtained as follows. The subject was asked to bite a dental

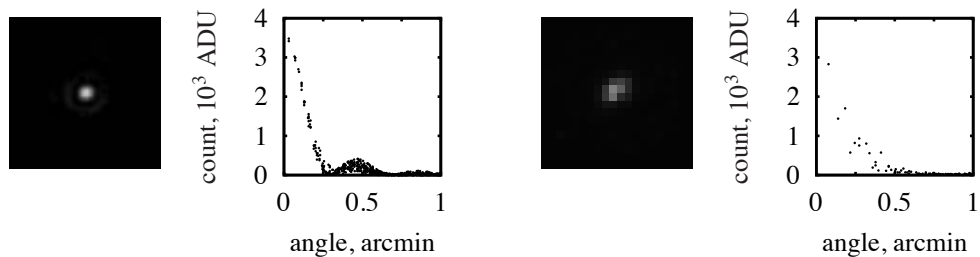


Fig. 2. Single pass PSF image of the system illumination (left) and observation (right) and the corresponding radial profile of intensity (CCD camera analog to digital counts, ADU). The image width is 4.0 arcmin.

impression attached to a three-axis translation stage. After alignment of the subject pupil, the amplitude of the tip, tilt, and defocus terms read by the WS were minimised by adjusting the incidence angle of the WS probing beam (tip, tilt) and by axially translating OL and the subject head (defocus). Then the subject was asked to blink, the AO loop was closed for 30 WS frames, the AO correction was frozen, and a double-pass PSF image was acquired. Following each exposure, the subject could blink normally and the DM was reset. After the third exposure, the subject removed his head from the instrument. For the Series 2, the series without AO correction, the operator waited 3 seconds after the blink before taking the exposure.

#### 2.4. Image analysis

For each frame, a constant bias level obtained from an unexposed corner of the CCD camera was subtracted. Then the centre of the light distribution was found by cross-correlation with a 1-arcmin half width at half maximum (HWHM) Lorentzian function,  $L(r) = cw/(w^2 + r^2)$ , where  $c$  is a constant and  $w$  is the HWHM. The distance (visual angle) from the centre of the light distribution to each pixel was computed and a plot of the radial intensity distribution (assuming rotational symmetry) was generated. A Lorentzian function was then fitted to this profile to obtain the HWHM of the double-pass PSF.

#### 2.5. Reconstruction of the double-pass PSF from the WS measurements

We obtained a series of single-pass PSF from the last 10 WS measurements preceding each frame acquisition by reconstructing the wavefront (least-square fit using 35 Zernike modes [24]), and by taking the square modulus of the field after propagation of the wavefront to the fundus, assuming an unit amplitude across the pupil. These 10 PSF were averaged and the double-pass PSF was obtained from the autocorrelation of this mean single-pass PSF [28] assuming a delta-correlated scattering at the retina [29]. The reconstructed double-pass PSF showed more radial variations than the measured double-pass PSF. Therefore, instead of plotting all pixel values, the mean radial profile was generated by averaging over 0.025 arcmin radial bins. The HWHM of these profiles was taken to be radial bin that held the value the closest to the half maximum.

For comparison, the double-pass PSF of a diffraction limited optical system was obtained by autocorrelation of the diffraction pattern (Airy disk). For our experimental setup this calculation yields a HWHM of the diffraction limited double-pass PSF of 0.19 arcmin.

#### 2.6. Tests of the method

In order to test the optical quality of the optical system including the presence of non-common pass errors, we measured the single-pass PSF of the illumination path and the single-pass PSF of

the observation path separately. First, the AO system is used to correct the aberrations measured by the wavefront sensor using a collimated beam instead of the subject's eye (point source whose light is collimated by a 80-mm focal length achromat). For the illumination path, the subject's eye was replaced by an achromatic lens with a focal length of 16 mm and the PSF was re-imaged using a 50x microscope objective. Figure 2 (left) shows an image of the single-pass PSF and its radial profile. The HWHM of this profile was found to be 0.146 arcmin using a fit of the function  $[2J_1(v)/v]^2$ . This value is very close to 0.143 arcmin, the HWHM of a diffraction limited PSF. As seen by the height of the first ring, some small aberrations are present. These aberrations are probably introduced by the achromatic lens used as artificial eye which is not part of the setup. This lens is working with an F-number of 2.4 compared to 15 for the lenses of the system. To measure the PSF of the observation path, the subject's eye was replaced by a plane wave (point source collimated by a 80-mm focal length achromat) and the PSF was recorded by the system CCD camera. The system was designed to sample the retinal image at the Shannon's critical frequency. The fine structures of the diffraction limited PSF are under sampled (Fig. 2 right). Most of the intensity is within a radius of 0.5 arcmin (fit gives a HWHM of 0.22 arcmin). The observation path is identical to the illumination path except for the beam splitter BS2 (peak to valley surface figure given at 63 nm) and for the lens L4.

To test whether the ocular aberrations during the acquisition of the double-pass PSF images was different from the aberrations measured at the end of the period of AO correction, we measured, in subject A, the wavefront aberrations during 30 frames of AO correction and during 30 additional frames with frozen corrections. The RMS wavefront aberration with frozen correction remained the same as the RMS wavefront aberrations obtained during the last 10 frames of AO correction.

### 3. Results

Without AO correction, the root mean square (RMS) wavefront aberration, without tip, tilt, and with minimised defocus, was 0.59, 0.36, 0.96, 0.41  $\mu\text{m}$  for subject A to D, respectively. A set of results obtained with AO correction is shown in Fig. 3. These data were obtained from one of the three measurement of the Series 1 at a focus position of 0  $\mu\text{m}$ . The first line shows the RMS wavefront aberrations obtained during AO correction and its average value over the last second of recording. This value is the RMS residual wavefront aberration after AO correction as measured by the wavefront sensor. The second line shows the measured double-pass PSF and the third line shows its radial profile with the Lorentzian fit and the HWHM in arcmin. The fourth line shows the reconstructed double-pass PSF and the fifth line shows its reconstructed radial profile with the extrapolated HWHM.

The mean residual wavefront aberrations over each measurement was  $0.087 \pm 0.016 \mu\text{m}$  (standard deviation) ranging from 0.052 to 0.127  $\mu\text{m}$  ( $N = 120$ ). The mean residual aberration for each subject (A to D) was 0.097, 0.085, 0.097, and 0.072  $\mu\text{m}$ .

Figure 4 shows the width of the double-pass PSF. The three measurements obtained at each focus depth were averaged. The black squares represent the width of the measured double-pass PSF for the Series 1 (fovea with AO correction). The black triangles show the width obtained for the Series 2 (fovea without AO correction). The open squares show the result of the Series 3 (at  $2^\circ$  of eccentricity with AO correction). The circles show the width of the reconstructed double-pass PSF of the Series 1 (black) and the Series 3 (white). And the horizontal dashed line represents the width of the diffraction limited double-pass PSF. The width of the measured double-pass PSF with AO correction (Series 1) shows a broad minimum around the axial position 0 and 30  $\mu\text{m}$  for subjects A, B, and C. The minimum measured width for subject D was the axial position 60  $\mu\text{m}$ . Without AO, the width of the double-pass PSF of subject C decreases monotonically from the axial position -60 to 60  $\mu\text{m}$ . This is almost certainly an effect



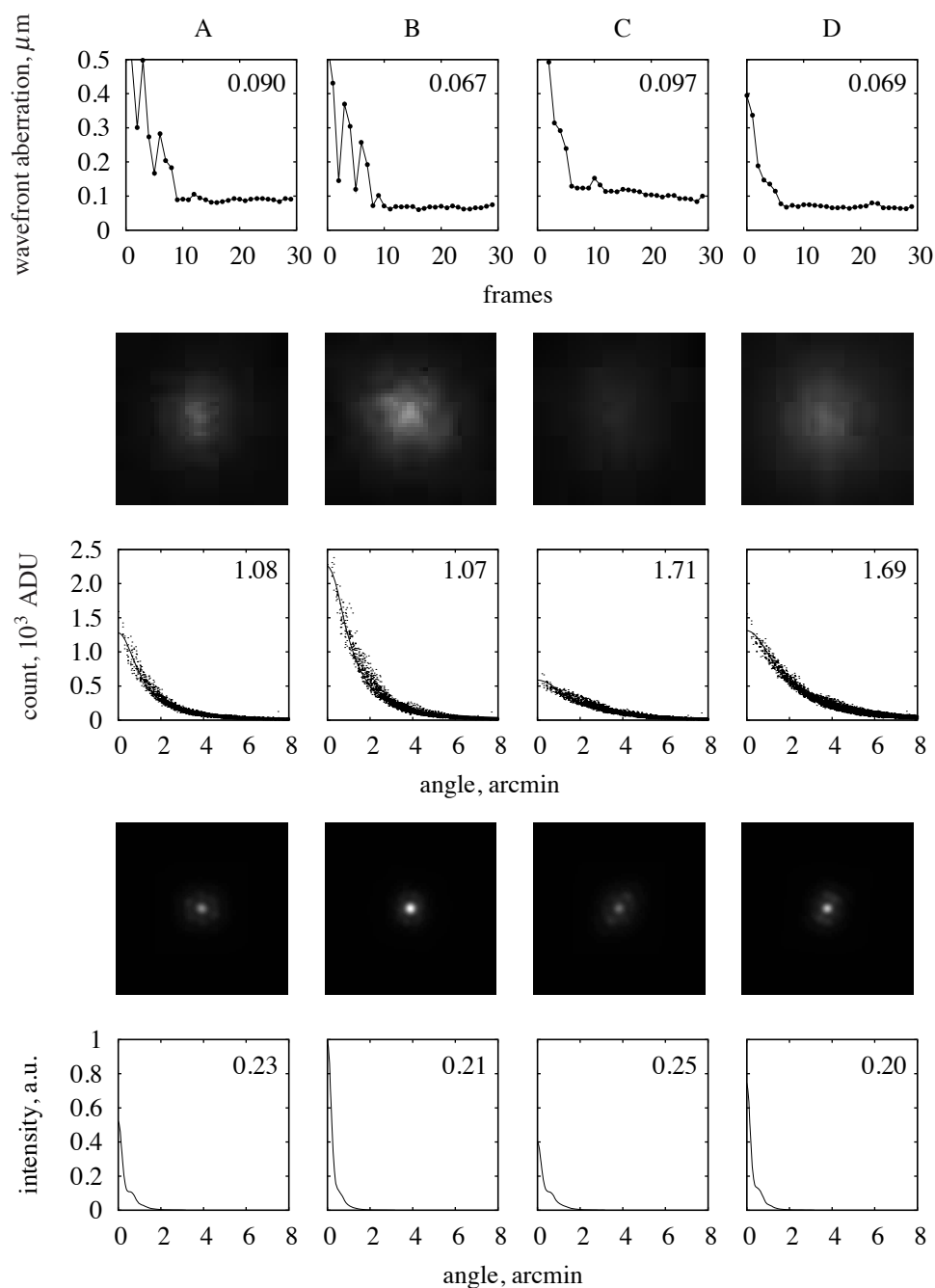


Fig. 3. Typical results obtained for the four subjects A to D (Series 1,  $0 \mu\text{m}$ ). The first line shows the RMS wavefront aberration during AO correction. The following lines show the measured double-pass PSF image (second), its radial profile of intensity with the Lorentzian fit (third), the reconstructed double-pass PSF (fourth) and its radial profile (sixth), all related to the WS data of the first line. All PSF images have a width of 8 arcmin.

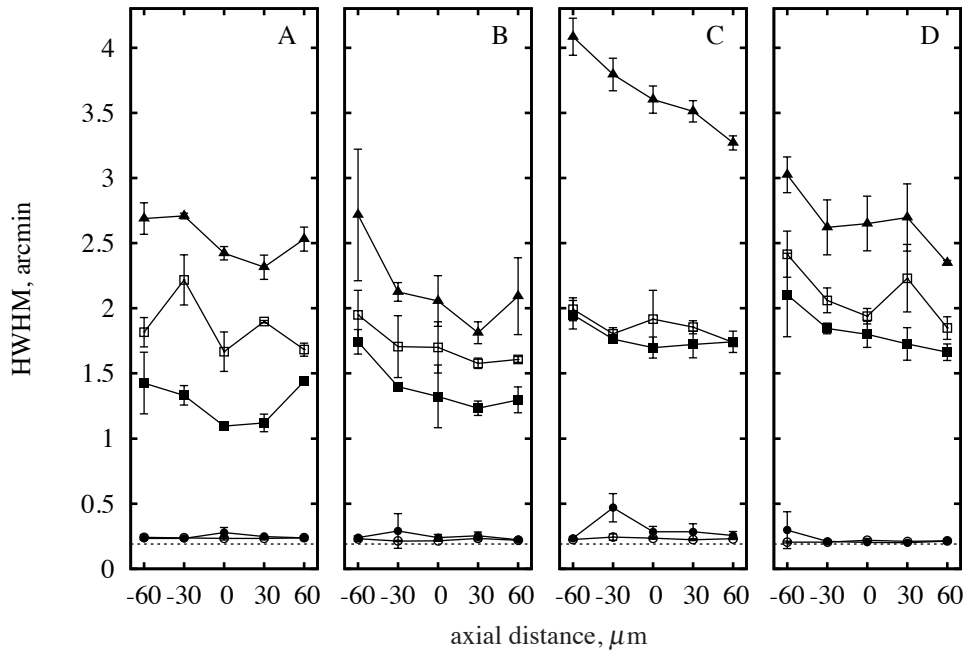


Fig. 4. HWHM of the double-pass PSF for the four subjects A to D and the three series; triangle at fovea without AO, black square at fovea with AO, open square at  $2^\circ$  of eccentricity with AO. The HWHM of the reconstructed double-pass PSF of the series with AO corrections are shown using circles. The black circle shows the data obtained at the fovea and open circle shows the data obtained at  $2^\circ$  of eccentricity. Error bars represent the standard deviation of the mean ( $N = 3$ ).

Table 1. Minimum HWHM in arcmin of the measured double-pass PSF obtained for each series and each subjects

Series	A	B	C	D
1	1.1	1.2	1.7	1.7
2	2.3	1.8	3.2	2.3
3	1.7	1.6	1.7	1.8

of uncorrected astigmatism.

The width of the minimum double-pass PSF obtained within each series is reported in Table 1. The following results can be noted. The width obtained with AO correction (Series 1) was always less than the width obtained without AO correction (Series 2). The width with AO correction was 48, 67, 53, and 74 % of the width without AO correction. The minimum width of the measured double-pass PSF for subject C and D is about 50 % larger than the width obtained for subject A and B. The width of the measured double-pass PSF is 5.8 and 6.3 times larger than the width of the diffraction limited double-pass PSF, for subject A and B, respectively, and it is 9 times larger for subject C and D. At  $2^\circ$  of eccentricity, the double-pass PSF were larger than the ones obtained at the fovea. This difference was larger for the subjects A and B than for the subjects C and D (Fig. 4 open and filled squares). The width of the reconstructed double-pass PSF after AO correction are all smaller than 0.5 arcmin (most around 0.2 arcmin), only marginally wider than the diffraction limit (Fig. 4).



#### 4. Discussion

In young subjects, using an annulus-shaped input pupil of 6.7-mm external diameter and 2.6-mm inner diameter, an unobstructed output pupil of 6.7-mm diameter, a wavelength of 543 nm, and careful focusing, we found that the width of the double-pass PSF after AO correction of the ocular aberrations is always smaller than the width of the double-pass PSF obtained in the same conditions but without AO correction. As expected, removing the ocular aberrations increases the compactness of the double-pass PSF. The width of this PSF, however, remains many times larger than either the width of the reconstructed double-pass PSF using the WS data or the width of the diffraction limited double-pass PSF.

Assuming that our wavefront sensor is not biased, the residual ocular aberrations after AO correction are too small to account for the measured double-pass PSF. Apart from the aberrations, the double-pass PSF can be degraded by scattering in the different ocular media, by contributions of out of focus reflecting surfaces, and by light diffusion behind the photoreceptors in the retinal pigment epithelium (RPE), in the choroid, and by the sclera.

The effect of scattering by the ocular media cannot be evaluated directly. Here we selected young subjects to minimise this contribution. The colour of the iris reflects the amount of melanin pigment within the choroid [30]. As, in our experiment, the width of the double-pass PSF measured in lightly pigmented eyes is about 50 % larger than the width of the double-pass PSF obtained in pigmented eyes, we can conclude that in lightly pigmented eye, there is a strong contribution from light scattered within the choroid. Absorption by haemoglobin and melanin is strong at 543 nm [30] but a small part of the PSF must be coming from the choroid even in a well pigmented eye. Geeraets *et al.* found in *ex vivo* preparation that about 5 % of the green light is transmitted through the RPE and the choroid of their most pigmented eye [31]. The retina at 2° of eccentricity is thicker than at the fovea and it comprises layers of cell and fibre not present at the fovea [32]. The measured double-pass PSF is larger at 2° of eccentricity than at the fovea. This difference may reflect the amount of light scattering within the retina. Retinal scattering is known and was measured subjectively by Vos and Bouman [33], is visible in the work of Zeimer *et al.* [34], and in the OCT signal from the inner retina. We can not rule out a difference in pigment density behind the retina at the two sites of measurements. Indeed, Weiter *et al.* showed that the concentration of melanin within the RPE peaks at the fovea [35]. Another difference which may influence the width of the double-pass PSF is the diameter of the cone photoreceptors. At the fovea, the cone photoreceptors are much smaller than at 2° of eccentricity [36].

We now compare our double-pass PSF with previous studies. In a previous report, we have shown that the width of short exposures double-pass PSF in two subjects after AO correction of the ocular aberrations were about 1 arcmin for a green probing beam and 3 arcmin for a red probing beam [37]. This result shows that the width of the double-pass PSF is not related to the 1 second exposure duration. Without AO correction and using 6-mm diameter pupil, early works obtained HWHM for the line spread function ranging from 3.1 to 6.6 arcmin using a polychromatic source [13,14]. This is larger than our results obtained without AO correction and it is most certainly due to the longitudinal chromatic aberration of the eye. Using a 6-mm diameter pupil and a monochromatic source emitting a 532 nm, Rodríguez and Navarro measured a double-pass PSF with an HWHM of 2.1 arcmin [19, Fig. 2a]. This value is within the range of values we obtained without AO correction. Using a 3.5-mm pupil and a wavelength of 633 nm, Liang and Westheimer showed HWHM of 0.9 and 1.7 arcmin for an x and y profile, respectively [16, Fig. 2a]. These values are similar in magnitude to the values we obtained through a large pupil after AO correction. The diffraction limit for a 3.5-mm pupil is about two times larger than the diffraction limit for the pupil size used in our study. Our results, however, are not diffraction limited. The largest contribution to the spread of the double pass PSF may

be from the light interaction with the fundus tissue. With a smaller pupil, the contribution from out of focus layers will be more compact than using a larger pupil. Another difference is that we blocked the central part of the illumination pupil to avoid back reflections and therefore we greatly reduced the guided contribution from the cone photoreceptors [38].

To achieve the narrowest light distribution at the fundus, there may be an optimum pupil size that balances the effect of the out of focus contributions and the effect of diffraction. Due to the shape of the light distribution in the double-pass PSF image, it appears difficult to obtain a tight concentration of light within about 1 arcmin. Our measurements show that the retina and deeper layers contribute to the double-pass PSF. This contribution is relatively larger in eyes with small amount of aberration and at measurement sites outside of the fovea. This result is in contradiction with the assumption needed to retrieve the single-pass optical transfer function from the double-pass PSF, and therefore, as Gorrand remarked before [39], caution is required in the interpretation of modulation transfer function of the eye obtained using the aerial image.

### **Acknowledgements**

We would like to thank Elie de Lestrang and Conor Leahy for their contribution. This work was supported by Science Foundation Ireland under grant No. 07/IN.1/I906.